

# MONITORING RAPIDLY EVOLVING LANDSCAPE FEATURES USING GROUND-BASED TIME-LAPSE PHOTOGRAPHY: A CASE STUDY FOR A PROGLACIAL ICING

K. Whitehead<sup>a\*</sup>, B. Moorman<sup>a</sup>, P. Wainstein<sup>a</sup>, A. Habib<sup>b</sup>

<sup>a</sup> Dept of Geography, University of Calgary, 2500 University Drive NW, Calgary, Alberta T2N 1N3  
\*kwhitehe@ucalgary.ca

<sup>b</sup> Dept of Geomatics Engineering, University of Calgary, 2500 University Drive NW, Calgary, Alberta T2N 1N3

**KEY WORDS:** Glacier, icing, time-lapse, ground-based photogrammetry, orthoimage

## ABSTRACT:

Two automated time-lapse cameras were set up to monitor the summer decay of the proglacial icing associated with Fountain Glacier. A series of photos were retrieved from each camera after two months. Initial determination of the camera orientation parameters was carried out using single photo resections. However variations in camera positions caused by melting of the surficial layers of permafrost meant that orientation parameters needed to be determined separately for each photograph. Final camera orientations were achieved by assuming the camera positions remained fixed and using twin reference points to adjust the rotational parameters. After successful determination of the camera parameters, a time series of orthoimages was generated from each camera location. These were subsequently used to obtain estimates of the rate of ice melt over the summer.

## 1. INTRODUCTION

Proglacial icings occur when subglacial water emerges onto a glacier's outwash plain and freezes successively in layers. Icings are relatively common hydro-cryological features associated with polythermal arctic glaciers. However, the proglacial icing associated with Fountain Glacier on Bylot Island is unique in the Canadian Arctic due to its size and perennial character. The main section of the icing is roughly 1.2 km in length by 300 m wide, and is several metres thick. Additionally, the icing does not entirely melt during the summer and some areas remain ice covered throughout the entire year.

This paper describes the application of a low-cost photogrammetric monitoring system which used time-lapse photography to monitor the seasonal decay of the icing over the summer of 2008. The primary objective of the project was to generate a series of orthoimages which could then be used to measure the changes in ice cover over the summer. While the results of this project were aimed at answering questions relating to glacial hydrology, such a system could easily be adapted to monitor a variety of evolving landscape features, thus potentially providing insight into processes as varied as beach erosion and stream migration.

## 2. STUDY AREA

Bylot Island is a mountainous island which is approximately 180 km in length by 100 km wide. The centre of the island is dominated by the rugged Byam Martin Mountain range, which forms the nucleus of a 4,500 km<sup>2</sup> icefield. Glaciers flow from this central hub towards the coast in a radial pattern. The location of Bylot Island is shown in Figure 1a.

Bylot Island is situated in the zone of continuous permafrost. It has a cold, dry climate, and an average temperature of -15°C (Irvine-Fynn et al. 2006). The average annual precipitation is less than 200 mm, with a maximum of 80 cm of snow falling in

the winter near the terminus of Fountain glacier (Moorman 2005).

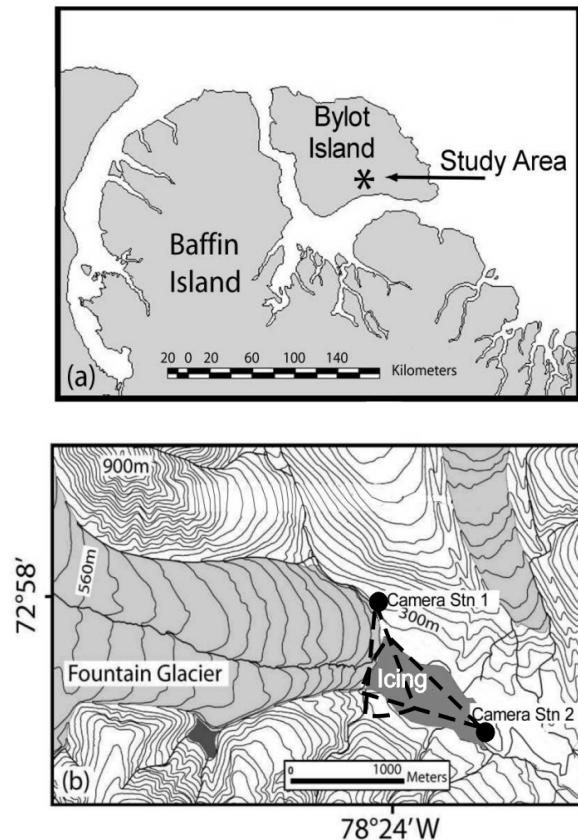


Figure 1a: Location of Bylot Island. Figure 1b shows a detailed view of the study area

\* Corresponding author

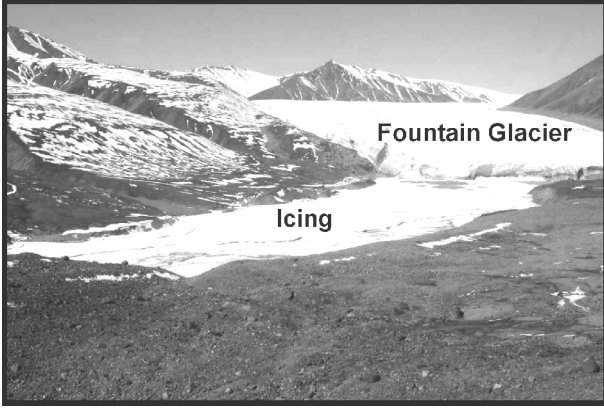


Figure 2: The terminus of Fountain Glacier with the icing in the foreground. View direction is from east to west

Fountain Glacier, which is officially listed as B26 in the Glacier Atlas of Canada (Inland Waters Branch 1969), lies to the South of the main icefield. It is about 15 km long and about 1.2 km wide close to its terminus, which is located at 72° 58' N, 78° 24' W. Evidence presented by Moorman (2003) and Wainstein et al. (2008) suggests that Fountain Glacier is polythermal in nature, consisting predominantly of cold ice, but having a temperate core. The icing occupies the proglacial floodplain immediately below the terminus of the glacier. The location of the icing with respect to Fountain Glacier is shown in Figure 1b and Figure 2.

It is believed that the size of the icing is a consequence both of the level of hydrological activity of Fountain Glacier itself, and also of the topography of the proglacial floodplain (Wainstein et al. 2008). The main section of the icing occupies the floodplain lying between the terminus of the glacier and a constriction 1.2 km further down the valley. Previous studies by Moorman (2003) and Wainstein et al. (2008) have linked the seasonal regeneration of the icing to the availability of a continuous year round supply of liquid water from beneath the glacier. Thus, the processes which cause the icing to build up and decay provide important information on the entire glacial hydrological system.

### 3. BACKGROUND

The monitoring of continuously evolving landscape features, such as those found in a proglacial environment, poses a number of challenges. While techniques such as repeat aerial photography and satellite image analysis can be used, the costs involved are high, and coverage may not be sufficiently frequent to provide the level of information required. For small areas which are changing rapidly, regular field surveys may provide a solution. However these are time consuming, and practical difficulties often arise when the area being investigated is remote and observations are required over an extended period of time.

A number of studies have applied ground-based photography and photogrammetric techniques to monitor changing landscapes in glacial and proglacial environments. Brecher and Thompson (1993) used ground-based photography to study the retreat of the Qori Kalis Glacier in the Peruvian Andes. Kaufman and Landstäedter (2004) used similar techniques to measure retreat rates for a small cirque glacier in the Austrian

Alps. Landstäedter & Kaufmann (2004) and Sanjosé & Lerma (2004) used close-range photogrammetric techniques to investigate the dynamics of rock glaciers.

To date, most photogrammetric studies in glacial regions have made use of intermittent hand held photography. Automated time-lapse photography was however used by Harrison et al. (1992) to monitor glacier speed during a surge of the West Fork Glacier in the Central Alaska Range. Speeds were estimated from the position of visible features on the glacier surface. Time-lapse photography was also used by Aschenwald et al. (2001) to monitor snow cover for a mountainous area in the Italian Tyrol over a four year period.

### 3.1 Theory

The relationship between object-space and image-plane coordinates is described mathematically by the collinearity equations. These equations are based on the assumption that a point in object space, the perspective centre of the camera lens, and the point's representation on the camera image plane lie on the same straight line. Leaving out lens distortion for the time being, these can be expressed as:

$$\begin{aligned} x_a &= x_p - c \frac{r_{11}(X_A - X_o) + r_{12}(Y_A - Y_o) + r_{13}(Z_A - Z_o)}{r_{31}(X_A - X_o) + r_{32}(Y_A - Y_o) + r_{33}(Z_A - Z_o)} \\ y_a &= y_p - c \frac{r_{21}(X_A - X_o) + r_{22}(Y_A - Y_o) + r_{23}(Z_A - Z_o)}{r_{31}(X_A - X_o) + r_{32}(Y_A - Y_o) + r_{33}(Z_A - Z_o)} \end{aligned} \quad (1)$$

Where  $x_a$  and  $y_a$  represent the image-plane coordinates of point A.  $x_p$  and  $y_p$  represent the coordinates of the principal point.  $c$  is the principal distance of the camera.  $X_A$ ,  $Y_A$ , and  $Z_A$  are the object-space coordinates of point A.  $X_o$ ,  $Y_o$ , and  $Z_o$  are the object-space coordinates of the perspective centre of the camera lens.  $r_{11}$  to  $r_{33}$  are elements of the 3x3 rotation matrix  $R$ . This matrix contains nine elements, but the only independent parameters are the three rotation elements  $\omega$ ,  $\phi$ , and  $\kappa$ .

After the camera has been calibrated to determine the relationship between the image plane and the camera lens, the collinearity equations may be used to transform 3D object space coordinates to 2D image plane (or photo) coordinates. If a digital elevation model (DEM) is available for the area then the reverse transformation can also be achieved, by projecting a ray of light from the photo point, through the perspective centre of the lens. Where this ray of light intersects the DEM the location of the point in 3D object space is defined. An orthoimage can then be created by repeating this process for every pixel of the image.

Exterior orientation parameters define the position and orientation of a camera in 3d object space. A camera has six degrees of freedom; three shifts, in X, Y, and Z, and three rotations  $\omega$ ,  $\phi$ , and  $\kappa$ , which correspond to rotations around the camera x, y, and z axes respectively. The main challenge for photogrammetric reconstruction is accurate determination of these parameters. To determine these, a process known as single photo resection is often used in ground-based photogrammetry.

If the positions of at least three ground control points are known in object space, and their corresponding positions are measured on the image, then the principle of collinearity can be used to uniquely define the position and orientation of the camera in space. Alternatively if the XYZ position of the camera is already known then the rotation parameters can be determined using only two points in space.

#### 4. METHODOLOGY

Two field visits were made to Bylot Island in May and June, and in August of 2008. On the first visit two camera stations were set up to view different sections of the icing. Camera 1 was set up to cover the section immediately below the glacier. This camera was set up looking south, across the icing. This part of the icing is topographically varied, and includes a number of ice-cored geomorphic features covering an elevation range of several metres.

Camera 2 was set up near the valley constriction at the eastern end of the icing and looked north west, up the length of the icing. Theoretically most of the icing was included in the field of view of this camera, but because of the location, the height difference between the camera station and the icing was only 22 m. This meant that further away objects showed very little vertical separation, so useful information could only be obtained for the eastern part of the icing, within 500 m of the camera. The locations of the two camera stations are shown in Figure 1b.

Each camera station consisted of a 10 MP Canon XTi Digital Rebel camera equipped with a 50 mm fixed zoom lens. Each camera was contained within a waterproof rugged enclosure and was powered by a solar array with two backup batteries. The timing of the photographs was controlled by a digital time-lapse controller.

Prior to departure for Bylot Island, a preliminary camera calibration was carried out. Time constraints meant that it was not possible to carry out a rigorous full field calibration. Instead a flat sheet calibration was carried out using PhotoModeler. While this is not ideal for high accuracy photogrammetric projects, the accuracy requirements for studying the icing were low. Errors of up to 5 m from the correct position could be tolerated. The same calibration was subsequently applied to both cameras.

The cameras were set up to take photographs every three hours over the period between the 10th of June and the 9th of August, when the imagery was retrieved. A full set of images was successfully retrieved from each camera. A subset of daily images was selected from each camera. Images from Camera 1 acquired at 12:20 pm each day were selected, since shadowing from the glacier was present on early morning images. For Camera 2, imagery acquired at 10:27 am was used in the analysis.

##### 4.1 Ground Control and DEM Survey

On the last day of the study, prior to image retrieval, six targets were set up on the surface of the icing, in areas which could be seen from both cameras. The targets consisted of a 60 cm red circle on a white background. Accurate positions were obtained for each of these targets, using real time kinematic GPS. Both camera positions were also measured by GPS at this time. The

targets were left set up for a full day, during which a number of images were acquired by each camera.

During both field visits, a complete survey of the icing was carried out, using real time kinematic GPS. This allowed DEMs to be generated for the icing surface at both the start and end of the study period. Since the icing extents were considerably smaller in August, the June DEM was used as a reference. Subtracting the two DEMs showed that in areas common to both DEMs, the ice had thinned by an average of 70 cm over the two month period. As a compromise 35 cm was subtracted from the June DEM over the area of the icing to provide the surface elevations to be used in the remainder of the study.

##### 4.2 Processing of Reference Images

The final image obtained from each camera station prior to image retrieval was used as a reference image. The six targets set up on the icing were visible on each reference image, giving six known target XYZ positions, as well as the known camera XYZ positions. The assumption was made that the GPS position of both the cameras and the targets were correct and these were considered to be fixed. A single photo resection was then carried out for each of the reference images in order to determine values for the three elements of rotation,  $\omega$ ,  $\phi$ , and  $\kappa$ .

	Camera 1		Camera2	
Error (pixels)	Y error	X error	X error	Y error
Target 1	5	0	1	0
Target 2	-1	0	2	0
Target 3	11	2.5	-0.5	-1
Target 4	2	2	0	-0.5
Target 5	-8	0	-0.5	0.5
Target 6	0.5	0	1	-1
RMS error	6.0	1.3	1.0	0.6

Table1: Comparison between measured and computed positions of targets for reference images from both cameras

The initial residuals from both single photo resections revealed that there was a significant scale error present in the photos taken by both cameras. It was assumed that this was due to an error in the calibrated principal distance, and this was adjusted by running repeated single photo resections in which the value for principal distance was adjusted to minimise the residuals at each control point. This resulted in the principal distance being adjusted to 51.3 mm for both cameras. The principal point offsets and the first order lens distortion parameter were also varied to see what effect these would have on the overall residuals. It was found that the effect of varying these parameters was minimal relative to the pixel size of 6  $\mu\text{m}$ , and in view of the low accuracy requirements of the study the original values for these parameters were used. The final residuals for the target positions from Camera 1 and Camera 2 are shown in Table 1.

The higher Y residuals for Camera 1 are believed to have been a consequence of the distribution of control points. This camera was situated relatively close to the targets, with no point further than 500 m away, and the points were widely distributed across the image. Camera 2 was around 800 m away from the targets, so that they occupied a relatively narrow band across the centre of the image, with little variation in the photo y direction. While this target configuration would not be acceptable for high accuracy applications, it was considered to be sufficiently good

to provide estimates for the camera rotation parameters, since the camera XYZ positions were fixed by GPS, rather than being determined during the single photo resection process.

### 4.3 Processing of Remaining Images

If no movement of either camera had occurred over the duration of the study then the exterior orientation parameters measured from the reference images could be applied to all images obtained from the same camera. However analysis of the photos showed that both cameras had undergone substantial movements over the summer, with Camera 2 especially badly affected. Comparison of photos taken at the start and end of the study showed that a shift of over 600 pixels had occurred in the Y direction for this camera. While the movements of each camera were too small to have a significant effect on its absolute XYZ position, the effect on the rotation parameters was significant and needed to be accounted for before the photos could be used in the analysis. It is believed that the shifts in camera position occurred as a result of melting of the surface permafrost layer. This is thought to have caused the rocks on which the cameras were set up to shift over the duration of the study.

Since control points were only available for the last few images taken by each camera it was not possible to reconstruct the imaging geometry of each photo by carrying out a series of single photo resections. Instead, a technique was developed using two widely spaced reference points on each image. The camera XYZ positions were assumed to have remained fixed over the duration of the survey, meaning that only the  $\omega$ ,  $\phi$ , and  $\kappa$  rotation parameters needed to be established for each photo. Two reference points were identified for each camera. These points were located on either side of the images at roughly the same distance from the image centre and could be reliably identified on all the photos used in the study.

Object space coordinates were then determined for each of the reference points. This was done by using photo coordinates measured off the oriented reference images. An approximate elevation was estimated for each point and object space coordinates were calculated by back projection. The coordinates defined the point at which a ray of light projected from the photo point through the perspective centre of the camera lens intersected with the given elevation of the point. The calculated coordinates did not reflect the true position of the reference points, since the elevation was only approximate. However, since the camera position was assumed to be fixed in X, Y, and Z the derived coordinates could be used to derive the rotation parameters relative to those of the reference image.

A program was written which used the measured line and column positions for the two reference points in each image to calculate the change in rotation parameters between the current and the reference image. The object space coordinates of the reference points were first converted to image plane coordinates using the collinearity equations with the original rotation parameters from the reference image. These row and column values were then compared with the measured values for the image concerned. This allowed corrections to be calculated sequentially for the  $\omega$ ,  $\phi$ , and  $\kappa$  values. New image plane coordinates were then calculated for the two reference points using the adjusted rotation parameters and the process was repeated until convergence was reached. When the calculated row and column positions agreed with the measured positions,

the values of  $\omega$ ,  $\phi$ , and  $\kappa$  were taken as final and written to the image.

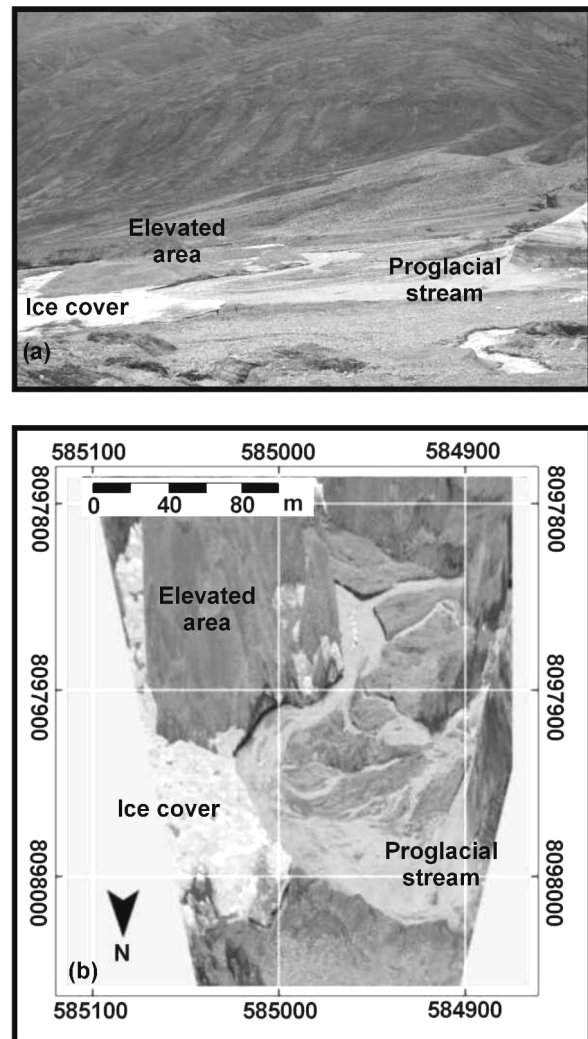


Figure 3a: Reference photo from Camera 1 on August 9<sup>th</sup>, and 3b: Orthoimage generated from this photo with a 100 m UTM 17 grid superimposed. Note how the elevated area to the left appears elongated as it is displaced away from the camera in the orthoimage

### 4.4 Orthoimage Generation

After the exterior orientation parameters had been calculated, an orthoimage was generated from each photograph. To do this the technique of back projection was again employed. The ray of light passing through each pixel and the perspective centre of the camera lens was extended until it intersected with the DEM. The pixel position in object space could therefore be calculated. By repeating this process for the entire image, a full orthoimage could be produced. The orthoimages generated from Camera 1 had a pixel size of 0.3m. Camera 2 covered a larger area, so orthoimages generated from this camera were assigned a pixel size of 0.5m.

As a final step the images were cropped to an appropriate window, so that only the area of interest was included. The reference image and derived orthoimage from Camera 1 are

shown in Figure 3, while the reference image and derived orthoimage from Camera 2 are shown in Figure 4.

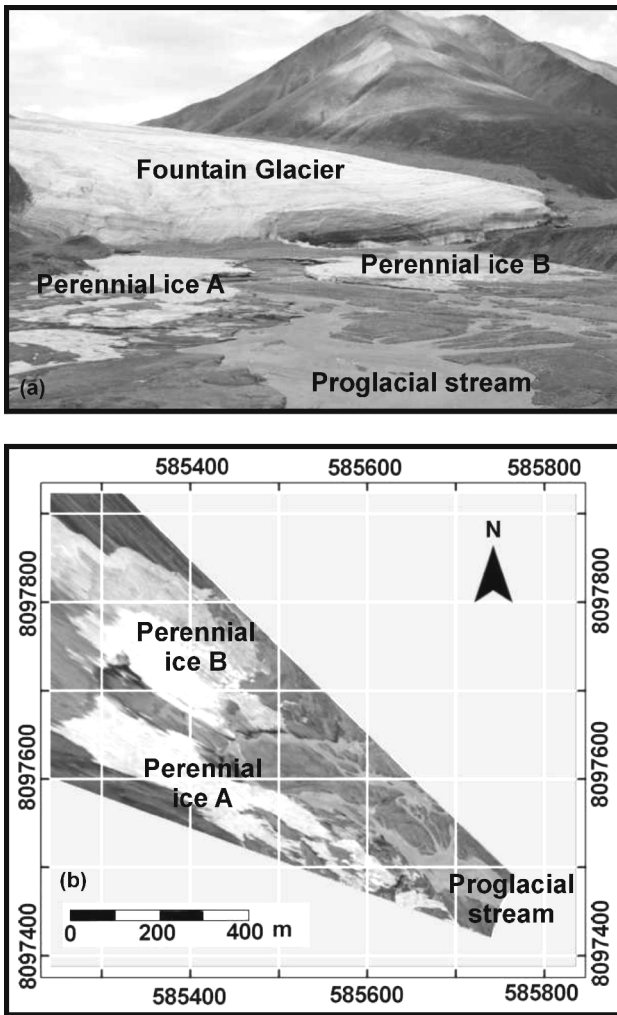


Figure 4a: Reference photo from Camera 2 on August 9<sup>th</sup>, and 4b: Orthoimage generated from this photo with a 100 m UTM 17 grid superimposed

#### 4.5 Verification

Check points were identified on each set of orthoimages in order to assess how well the process of determining exterior orientation parameters and generating orthoimages had worked. The requirement to use points which were not located on the ice surface and which were unambiguous meant that only one suitable point could be found for each set of orthoimages. A point was chosen for Camera 1 which could be reliably identified over the 43 day period prior to the retrieval of the images, and for Camera 2 a point was selected which could be identified consistently on images acquired over the last 38 days of the project.

### 5. RESULTS

Comparison of the check point coordinates over time revealed that the orthoimages generated from Camera 2 showed much greater consistency than those generated from Camera 1. Over the 38 days the point position was measured for Camera 2 it

showed a maximum variation of 4 m in easting and 2 m in northing, compared to the position measured on the orthoimage derived from the reference image. The RMS variation over this period was 1 m in easting and 0.8 m in northing. During this period, the camera rotation elements were continuously changing. On one occasion the measured camera y coordinates experienced a jump of over 600 pixels over a two day period, yet the output orthoimages remained stable, suggesting that the rotational parameters had been correctly derived.

The orthoimages obtained from Camera 1 showed a much greater variation. Over the 43 days the check point was measured there was a maximum variation of 1.5 m in easting and 7.8 m in northing. The RMS variation over this period was 0.57 m in easting and 3.5 m in northing. Unlike the measurements obtained for Camera 2, which showed only random variations, there appeared to be a definite trend occurring over time, with the apparent position of the check point moving towards the camera over time. This occurred in spite of the fact that the original photos obtained from Camera 1 appeared to have varied little over the study period.

### 6. DISCUSSION

While the method outlined above is easy to implement and offers many advantages for low accuracy monitoring applications, some problems were observed in its implementation. The script which was used to determine the rotation parameters of each individual image worked well, however some scale variations were noted between the two reference points. This was most apparent for Camera 2, after the photo y values of the two reference points changed by over 600 pixels over a two day period, as a result of a large  $\omega$  rotation. When this occurred, the distance between the two reference points increased by several pixels. This scale variation is believed to be a result of residual lens distortion, since the new positions of the reference points were further from the image centre and therefore would be subject to more lens distortion.

The section of the icing covered by Camera 1 included a number of glacio-morphic features, many of which were several metres high. The DEM used was compiled from points on the icing surface only and did not include these features. Therefore, these elevated features were not represented correctly on the output orthoimages. When the camera is looking downward, features which are higher than the elevation given by the DEM will be displaced away from the camera, while those lower than the DEM elevation will be displaced towards the camera. This effect can clearly be seen for elevated areas in Figure 3. Since the level of the icing itself changed relatively little, and since the ice surface was relatively flat, it was still possible to make reliable measurements over the ice covered sections of this area.

The section of the icing covered by Camera 2 was relatively flat. However, the camera was located only 22 m above the surface of the icing, which meant that there was very little vertical angular separation between features in the middle distance. Because of the flat nature of the icing, it was possible to still create a realistic orthoimage at distances of up to 500 m. However at this distance, a height variation of only a few centimetres will lead to considerable displacement in the direction towards or away from the camera. This phenomenon could be clearly seen when looking at the time series of the ice covered areas. As the ice level dropped, the ice covered area was displaced towards the camera, whereas the bare area

remained at a constant distance, since its level remained unchanged. To correct for this effect, it would be necessary to use a separate DEM for each photo.

The use of check points can only give an approximate indication as to the reliability of the orthoimages. To properly verify their accuracy, it would be desirable to have a number of check points scattered throughout each set of orthoimages. This was not possible, since it was extremely difficult to identify any points in areas which were not ice covered, and most ice free areas on the changed over the duration of the project as the floodplain was reworked by glacio-fluvial activity.

The quality of the output orthoimages could have been improved in a number of ways. If a high quality DEM were available from LIDAR, or from a detailed ground survey, this would have improved the quality of the output orthoimages considerably. Having good elevation information would considerably reduce the displacement of high elevation areas away from the camera. It is believed that unaccounted for elevation variations may partially account for the variation observed in orthoimages generated from Camera 1.

Another way to minimise distortions in the output images would be to change the viewpoint. If the area of the icing were viewed from further away at a steeper vertical angle variable relief displacement effects would be considerably reduced. For a relatively flat area such as the icing, such a viewpoint would improve the quality of the orthoimages considerably. The ideal location to set up a camera for this study would have been on the ridge to the North of the icing. From this position, the quality of the output orthoimages would have been relatively insensitive to variations in the DEM. Practical constraints, including the need to regularly check the cameras after installation, ruled out the possibility of installing a camera on the ridge for this project.

## 7. CONCLUSION

The time-series of orthoimages produced for each camera station provided a valuable record, showing how the icing changed throughout the summer. By analysing these images the changing ice extents could be mapped. One of the most revealing ways to interpret the information is to put the series of orthoimages for each camera together as a movie. When this was done, the patterns of melting and ice break up over the summer could be clearly seen, giving important insight to further the understanding of the glacio-hydrological processes involved in the thermal erosion of the icing.

In an ideal case, variations would not occur in camera positions. In practice however there are a number of factors which can cause the rotation parameters of the camera to change. This study describes a method which can be used to re-establish the unique rotation parameters for each image, using two reference points. While the absolute accuracy requirements for this study were low, the procedure could easily be modified by using a higher accuracy DEM, permanent control points, and better calibrated cameras to give more accurate results.

## REFERENCES

Aschenwald, J., K. Leichter, E. Tasser and U. Tappeiner, 2001. Spatio-Temporal Landscape Analysis in Mountainous Terrain

by Means of Small Format Photography: A Methodological Approach. *IEEE Transactions on Geoscience and Remote Sensing*, Vol 39(4), pp. 885-893.

Brecher, H. H. and L. G. Thompson, 1993. Measurement of the Retreat of Qori Kalis Glacier in the Tropical Andes of Peru by Terrestrial Photogrammetry. *Photogrammetric Engineering and Remote Sensing* Vol 59(6), pp.1017-1022.

Harrison, W. D., K. A. Echelmeyer, D. M. Cosgrove and C. F. Raymond, 1992. The Determination of Glacier Speed by Time-Lapse Photography under Unfavourable Conditions. *Journal of Glaciology* Vol 38(129), pp.257-265.

Inland Waters Branch, 1969. *Atlas of Canada: Bylot Island Glacier Inventory: Area 46201*, Department of Energy, Mines and Resources, Ottawa.

Irvine-Fynn, T. D. L., B. J. Moorman, J. L. M. Williams and F. S. A. Walter, 2006. Seasonal Changes in Ground-Penetrating Radar Signature Observed at a Polythermal Glacier, Bylot Island, Canada. *Earth Surface Processes. Landforms* Vol 31, pp.892-909.

Kaufmann, V. and R. Landstäedter, 2004. Documentation of the Retreat of a small Debris-Covered Cirque Glacier (Goessnitzkees, Austrian Alps) by Means of Terrestrial Photogrammetry. *4th ICA Mountain Cartography Workshop*, Vall de Núria, Catalonia, Spain.

Landstäedter, R. and V. Kaufmann, 2004. Change Detection of a Mountain Slope by Means of Ground-Based Photogrammetry: A Case Study in the Austrian Alps. *4th ICA Mountain Cartography Workshop*, Vall de Núria, Catalonia, Spain.

Moorman, B., 2003. Glacier-permafrost hydrology interaction, Bylot Island, Canada. *Permafrost: 8th International Conference*. A.A. Balkema Publishers, pp. 783 - 788.

Moorman, B. J., 2005. Glacier-permafrost hydrology interconnectivity: Stagnation Glacier, Bylot Island, Canada. *Cryospheric Systems. Glaciers and Permafrost* (Special Publication 242): pp. 63-74.

Sanjosé, J. J. and J. L. Lerma, 2004. Estimation of Rock Glacier Dynamics by Environmental Modelling and Automatic Photogrammetric Techniques. XXth ISPRS Congress, Istanbul, Turkey, pp. 905-909

Wainstein, P., B. Moorman and K. Whitehead, 2008. Importance of Glacier - Permafrost Interactions in the Preservation of a Proglacial Icing: Fountain Glacier, Bylot Island, Canada. *Ninth International Conference on Permafrost*, Fairbanks, Alaska, 2, pp.1881-1886

## ACKNOWLEDGEMENTS

This work was supported by grants and in-kind contributions from the Natural Sciences and Engineering Research Council of Canada (NSERC), the Polar Continental Shelf Program (PCSP), Indian and Northern Affairs Canada, Parks Canada and Alberta Ingenuity. Logistical support was provided by Parks Canada.